A THEORETICAL QUANTUM STUDY OF THE ELECTRONIC PROPERTIES OF MENTOXY DICHLORO PHOSPHOROUS ($C_{10}H_{19}OPCl_2$)

AMIR LASHGARI[a], SHAHRIAR GHAMAMI[a], M. GOVINDARAJAN[b], GUILLERMO SALGADO-MORÁN[c], PAOLA MONTES ROMERO[c], LORENA GERLI CANDIA[d]*

[a]*Department of Chemistry, Faculty of Science, Imam Khomeini International University, Qazvin, 34148-96818,*
[b]*Department of Physics, Avvaiyar Government College for Women (AGCW), Karaikal, Puducherry 609602, India*
[c]*Departamento de Ciencias Químicas, Facultad de Ciencias Exactas, Universidad Andrés Bello, Sede Concepción, Concepción, Chile*
[d*]*Departamento de Química Ambiental, Facultad de Ciencias, Universidad Católica de la Santísima Concepción, Concepción, Chile*

ABSTRACT

A theoretical quantum study of the organophosphorus compound with formula $C_{10}H_{19}OPCl_2$ (MEPCL2) was carried out. The results of the calculations show excellent agreement between experimental and computed frequencies evaluated at the B3LYP/6-311++G(d,p) level of theory. A study of the electronic properties, such as excitation energies and wavelengths were performed employing the time-dependent DFT (TD-DFT) method. Global a chemical reactivity of MEPCL2 was analyzed through global reactivity descriptors, while its local reactivity was analyzed by mean maps of the electrostatic potential. Also, the orbital energies values suggest that a charge transfer is occurring within the molecule.

Keywords: Phosphorous compound; DFT; HF; HOMO-LUMO.

1. INTRODUCTION

Organophosphorus compounds are of great interest because many biological processes such as energy transfer, bone synthesis, amino acid synthesis, among others are related to them[1]. Consequently, it is not so strange that many researchers are studying them to understand their role in biological systems[2-4]. Moreover, phosphorus compounds are employed in numerous synthetic procedures to manufacture detergents, fertilizers, pesticides, toxic industrial phosphate esters, natural products, among others[5,6].

Recently, mentoxy dichloro phosphorous ($C_{10}H_{19}OPCl_2$) (MEPCL2) was synthesized from the reaction of 2-(2-propyl)-5-methyl-1-cyclohexanol (menthol) with PCl_3. This new organophosphorus compound exhibits a maximum absorbance at 227 nm, this value indicates that MEPCL2 has important absorption properties in the visible region of the electromagnetic spectra, by which may useful in the fabrication of photovoltaic devices. However, to the best of our knowledge, there is no information about the electronic properties and the chemical behavior of MEPCL2. Thus, it is necessary to get a deeper knowledge about this compound, to identify its potential uses and applications. In this sense, the evaluation of these properties may result expensive and complicated from the experimental point of view. However, the accepted theories of the quantum chemistry provide advantages to analyze the electronic properties and reactivity of molecules reliably[7]. Therefore, in the present work, we perform a computational and theoretical quantum study about the electronic properties and chemical reactivity exhibited by MEPCL2. We consider that this kind of study will contribute to getting a better understanding of the chemical behavior of this new organophosphorus compound.

2. METHODOLOGY

The entire quantum chemical calculations have been performed at HF and DFT (B3LYP) methods with 6-311++G(d,p) basis sets using the Gaussian 03W program[8]. The optimized structural parameters have been evaluated for the calculations of vibrational frequencies by assuming Cs point group symmetry. At the optimized geometry for the title molecule no imaginary frequency modes were obtained, therefore there is a true minimum on the potential energy surface was found. As a result, the unscaled calculated frequencies, reduced masses, force constants, infrared intensities, and depolarization ratios are obtained. In order to fit the theoretical wavenumbers to the experimental, the scaling factors have been introduced by using a least square optimization of the computed to the experimental data. Vibrational frequencies are scaled as 0.9067 for HF and 0.961 for B3LYP[9] to account for systematic errors caused by basis set incompleteness, neglect of electron correlation and vibrational anharmonicity. The assignments of the compound are calculated by using VEDA program[10].

The electronic absorption spectra for optimized molecule calculated with the time-dependent DFT (TD-DFT) at B3LYP/6-311++G(d,p) level in gas phase and solvent (Acetonitrile, chloroform, and water). The ^{13}C nuclear magnetic resonance (NMR) chemical shifts of the molecule were calculated by the gauge-independent atomic orbital (GIAO) method in $CDCl_3$ and compared with experimental results.

3. RESULTS AND DISCUSSION

3.1. Molecular geometry

The geometry optimization of MEPCL2, see Fig. 1, was carried out at the HF/6-311++G(d,p) and B3LYP//6-311++G(d,p) levels of theory.

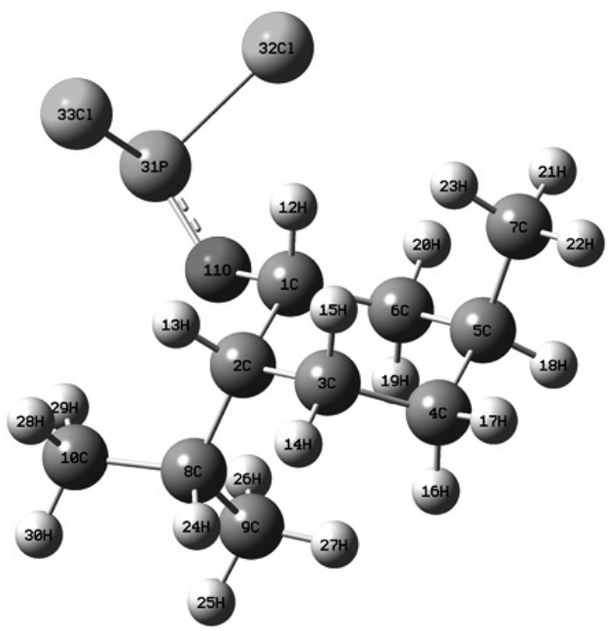

Fig. 1. Optimized molecular structure of MEPCL2 with atom numbering.

No imaginary frequencies were obtained, which ensures us that each gradient optimization located corresponds to true minimum energy on the energy potential surface. The selected optimized structural parameters, bond lengths and bond angles of the title compound are reported in Table 1. From

e-mail: loregerli@ucsc.cl

this table, it is possible to observe that the bond lengths and bond angles values calculated at the HF/6-311++G(d,p) and B3LYP/6-311++G(d,p) levels of theory compare favorably well with those reported in the literature. A linear fit of the optimized data, see Fig. 2 suggests that the bond lengths values calculated at the HF/6-311++G(d,p) level is slightly better than the geometry obtained at the B3LYP/6-311++G(d,p) level. However, this difference is in the order of the error associated with the resolution of the wavefunction when numerical algorithms are employed. Thus, no significant differences were obtained, which is indicative that the electronic correlation has a little effect on the molecular geometry of the MEPCL2.

Table 1. Selected optimized parameters of MEPCL2

Bond length	HF/ 6-311++ G(d,p) (Å)	B3LYP/6-311++ G(d,p) (Å)	Experimental Value (Å)[7]	Bond angle	HF/ 6-311++ G(d,p) (°)	B3LYP/ 6-311++ G(d,p) (°)	Experimental Value (°)[7]
C1-H12	1.083	1.093		H12-C1-O11	107.0	106.4	
C2-H13	1.085	1.095	0.970	H13-C2-C3	105.6	105.8	
C3-H14	1.086	1.094	0.970	H14-C3-H15	105.8	105.7	108.1
C3-H15	1.088	1.096	0.970	H15-C3-C4	108.9	109.0	109.5
C4-H16	1.086	1.094	0.970	H16-C4-C5	109.2	109.3	109.5
C4-H17	1.087	1.095	0.970	H17-C4-H16	106.2	106.1	108.1
C5-H18	1.088	1.096	0.970	H18-C5-C7	106.6	106.9	107.9
C6-H19	1.082	1.090	0.970	H19-C6-C1	109.2	109.2	109.3
C6-H20	1.085	1.094	0.970	H20-C6-H19	106.8	106.9	107.9
C7-H21	1.086	1.094		H21-C7-H23	107.4	107.4	
C7-H22	1.087	1.094		H22-C7-H21	107.7	107.8	
C7-H23	1.086	1.093		H23-C7-H22	107.4	107.3	
C8-H24	1.088	1.098		H24-C8-C10	106.0	106.2	
C9-H25	1.087	1.094		H25-C9-H27	107.1	107.1	
C9-H26	1.084	1.093		H26-C9-H25	107.5	107.3	
C9-H27	1.083	1.091		H27-C9-H26	108.5	108.4	
C10-H28	1.086	1.094		H28-C10-H30	107.7	107.7	
C10-H29	1.084	1.092		H29-C10-H28	108.0	108.0	
C10-H30	1.087	1.094		H30-C10-H29	107.6	107.7	
C1-C6	1.526	1.528	1.534	C4-C3-C2	114.6	114.5	110.5
C4-C3	1.531	1.535	1.521	C2-C1-C6	115.7	115.9	110.8
C2-C1	1.537	1.540	1.532	C7-C5-C6	112.6	112.5	
C7-C5	1.537	1.538		C9-C8-C2	118.4	118.1	
C9-C8	1.534	1.539		C10-C8-C9	110.1	110.0	
C5-C4	1.535	1.543	1.523	C6-C5-C4	109.1	109.2	111.7
C10-C8	1.539	1.540		C8-C2-C3	107.7	107.6	
C6-C5	1.536	1.546	1.525	O11-C1-C6	113.9	113.8	
C3-C2	1.546	1.552	1.513	P31-O11-C1	132.3	130.1	
C8-C2	1.447	1.567		Cl32-P31-O11	102.4	102.8	
O11-C1	1.563	1.576		Cl33-P31-Cl32	98.4	98.5	
P31-O11	1.568	1.600					
Cl32-P31	2.093	2.141					
Cl33-P31	2.093	2.141					

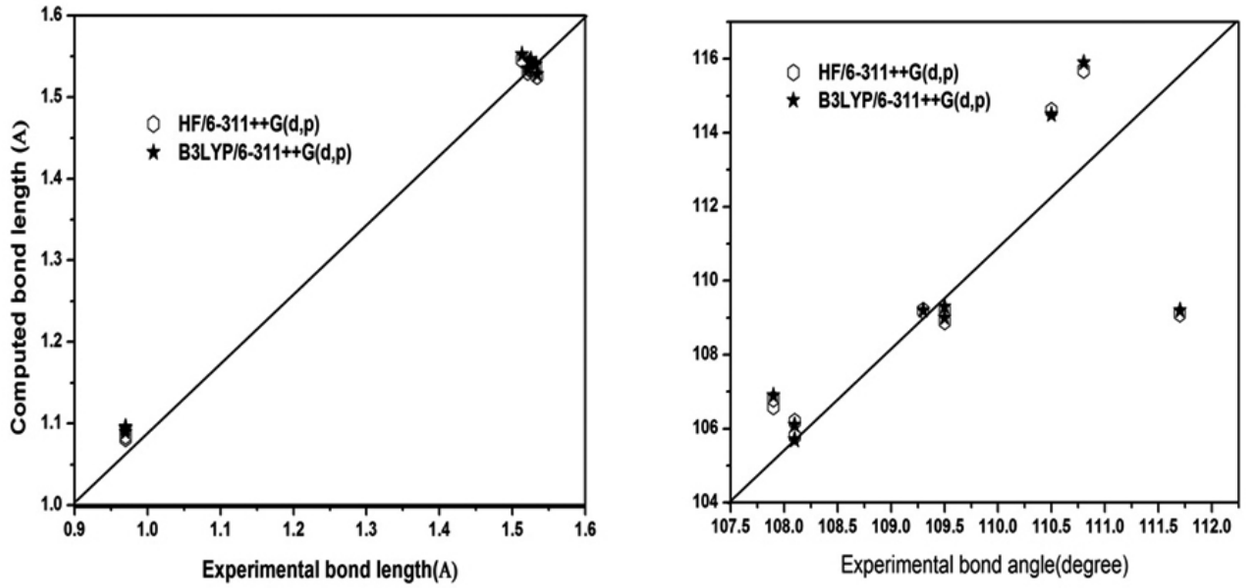

Fig. 2. Linear fit bond length and bond angle.

3.2. Vibrational analysis

The number of potential active fundamental vibrations of a non-linear molecule which contains N atoms is equal to (3N-6), apart from three translational and three rotational degrees of freedom. Therefore, MEPCL2 molecule has 33 atoms with 93 normal modes of vibrations. In the present work, we have done a detailed vibrational assignment of the experimental wavenumbers reported in a previous work, through the comparison with theoretically scaled wavenumbers evaluated at the HF/6-311++G(d,p) and B3LYP/6-311++G(d,p) levels of theory. In order to fit the theoretical wavenumbers to the experimental data, the scaling factors have been introduced by using a least square optimization of the computed to the experimental data. Vibrational frequencies are scaled as 0.9067 for HF and 0.961 for B3LYP[10] to take into account the systematic errors caused by basis set incompleteness, neglect of electron correlation, in the case of HF calculations, and vibrational anharmonicity. The assignments of the compound are calculated by using VEDA program[10]. The calculated experimental and scaled frequencies using HF and DFT (B3LYP) with the 6-311++G(d,p) basis set are listed in Table 2.

Table 2. Detailed vibrational assignments of observed and computed wavenumbers of MEPCL2.

Modes species	Exp[a]	HF/6-311++G(d,p)		B3LYP/6-311++G(d,p)			Mode description [b]
	Infrared[7]	unscaled	scaled	I_{IR}	unscaled	scaled	
1. A′		3266	2962	31.7	3111	2989	γCH cyclohexane
2. A′		3255	2951	21.4	3109	2988	γCH cyclohexane
3. A′		3243	2941	24.1	3104	2983	γCH cyclohexane
4. A′		3237	2935	37.4	3097	2976	γCH cyclohexane
5. A′		3227	2926	44.0	3086	2966	γCH cyclohexane
6. A′		3224	2923	52.6	3085	2965	γCH cyclohexane
7. A′	2957 vs	3219	2918	16.5	3081	2961	γCH cyclohexane
8. A′		3216	2916	64.0	3064	2944	γCH cyclohexane
9. A′		3208	2908	9.3	3056	2937	γCH cyclohexane
10. A′		3205	2906	15.4	3053	2934	γCH cyclohexane
11. A′	2928 vs	3198	2899	33.4	3052	2933	γCH_3 sym
12. A′		3189	2892	11.1	3034	2916	γCH_3 sym
13. A′		3175	2879	52.9	3031	2913	γCH_3 sym
14. A′		3173	2877	35.7	3030	2912	γCH_3 sym
15. A′		3163	2867	33.0	3026	2908	γCH_3 sym
16. A′		3162	2867	15.4	3024	2906	γCH_3 sym
17. A′		3159	2864	6.7	3017	2899	γCH_3 sym
18. A′		3155	2860	16.6	3012	2894	γCH_3 sym

19. A′		3145	2851	22.0	2994	2877	γCH_3 sym
20. A′	1456 m	1644	1490	9.0	1519	1459	γC-C ring
21. A′		1637	1484	10.5	1515	1456	γC-C ring
22. A′		1630	1478	3.9	1512	1453	γC-C ring
23. A′		1627	1475	19.4	1506	1447	βCH
24. A′		1621	1470	3.3	1502	1444	γC-C
25. A′		1620	1469	2.2	1500	1441	γC-C ring
26. A′		1617	1466	9.9	1494	1436	γC-C
27. A′		1610	1459	1.4	1488	1430	γC-C ring
28. A′		1607	1457	0.5	1485	1427	γC-C ring
29. A′	1388 m	1560	1415	8.6	1431	1375	βCH
30. A′	1370 m	1555	1410	13.8	1422	1366	γC-O
31. A′		1546	1402	1.9	1418	1363	γC-C
32. A′		1538	1394	1.6	1409	1354	γC-C
33. A′	1348 w	1532	1389	8.5	1401	1347	βCH
34. A′		1521	1379	1.0	1396	1341	βCH
35. A′	1330 w	1512	1371	1.9	1384	1330	βCH
36. A′		1500	1360	2.2	1375	1322	βCH
37. A′		1493	1354	0.5	1368	1315	βCH
38. A′		1480	1342	2.3	1361	1308	βCH
39. A′		1478	1341	3.4	1358	1305	βCH
40. A′		1457	1321	1.6	1330	1278	βCH
41. A′		1447	1312	7.3	1325	1274	βCH
42. A′		1432	1298	4.3	1303	1253	βCH
43. A′	1224 m	1381	1252	4.2	1272	1222	βCH m
44. A′		1358	1231	0.9	1258	1209	βCH m
45. A′	1180 m	1305	1183	3.0	1205	1158	βCH m
46. A′		1283	1164	0.5	1188	1142	βCH
47. A′		1277	1158	1.9	1173	1128	βCH m
48. A′		1255	1138	3.7	1155	1110	βCH m
49. A′	1060 m	1193	1082	4.0	1109	1066	βCH m
50. A′		1188	1077	0.8	1100	1057	βCH m
51. A′		1174	1065	2.4	1089	1046	βCH m
52. A′		1140	1034	4.7	1054	1013	βCH m
53. A′	992 s	1128	1023	5.3	1042	1001	γP-O
54. A′	974 s	1120	1015	38.5	990	951	βCCC ring
55. A′		1067	968	3.2	988	950	βCCC
56. A′	934 m	1066	967	455.3	973	935	βCCC ring
57. A′		1043	946	30.6	967	929	βCCC
58. A′		1032	935	13.2	959	921	βCCC ring
59. A′		1021	926	2.6	948	911	βCCC
60. A′		997	904	0.7	929	893	βCCO
61. A′	879 w	979	887	2.8	905	870	βPOC
62. A′		937	850	3.2	872	838	βPOCl
63. A′	825 w	929	842	18.6	862	829	βClPCl
64. A″	770 vw	857	777	15.6	792	761	φCH

65. A″		829	752	4.3	774	744	φCH
66. A″		794	720	1.6	745	716	φCH
67. A″		723	656	3.1	670	644	φCH
68. A″	586 vw	646	585	2.8	604	581	φCH
69. A″	495 w	582	527	1.6	543	522	φCH
70. A″	447 vw	535	485	64.7	482	463	γP-Cl
71. A″		499	452	18.9	440	423	γP-Cl
72. A″		469	425	108.2	428	411	φCH m
73. A″		457	414	40.4	414	398	φCH m
74. A″		454	411	15.4	411	395	φCH m
75. A″		424	384	3.5	390	374	φCH m
76. A″		416	377	3.3	381	366	φCH m
77. A″		387	351	3.7	349	335	βClPCl
78. A″		368	334	2.8	338	325	φCH m
79. A″		347	314	1.9	319	306	φCH m
80. A″		318	289	0.2	288	277	φCH m
81. A″		308	280	0.3	280	270	φCCC ring
82. A″		247	224	0.4	231	222	φCCC ring
83. A″		234	212	0.0	221	212	φCCC
84. A″		233	211	0.2	214	206	βClPCl
85. A″		222	201	0.4	196	188	φPOCC
86. A″		204	185	0.5	185	178	φClPOC
87. A″		180	163	1.7	163	157	φCCC
88. A″		142	129	1.6	129	124	φCCC
89 A″		90	82	1.1	86	83	φClOClP
90 A″		79	72	0.5	70	67	φCCC
91 A″		60	55	0.2	50	48	φCCC
92 A″		57	52	0.2	46	44	φCCC
93 A″		34	31	0.2	26	25	φPCCl

[a] s: strong; vs: very strong; m: medium; w: weak; vw: very weak. [b] γ: stretching; β: in-plane bending; φ: out-of-plane bending; I_{IR}: IR intensity.

3.2.1 Cyclohexane ring vibrations

Cyclohexyl ring in MEPCL2 contains three methylene (CH_2) groups, each group has six modes of vibration namely asymmetric and symmetric stretching, scissoring, rocking, wagging and twisting modes. In general, in cyclohexane, the CH_2 stretching vibrations are usually observed below 3000 cm^{-1} [11]. The asymmetric CH_2 stretching vibration generally observed in the region is 3000–2900 cm^{-1} while the CH_2 symmetric stretch is between 2900 and 2800 cm^{-1} [12,13]. In MEPCL2, the calculated wavenumbers at 2934, 2933, 2916, 2913, 2912, 2908 and 2906 cm^{-1} are attributed to asymmetric CH_2 stretching vibrations, while the symmetric CH_2 stretching wave numbers are calculated as 2899, 2894 and 2877 cm^{-1} at the B3LYP/6-311++G(d,p) level of theory. One stretching vibration of cyclohexyl ring is observed in MEPCL2, as very strong band at 2928 cm^{-1} in FT–IR spectrum. The vibrations due to aromatic C–H in-plane bending are observed in the region 1000–1300 cm^{-1} [14]. For this compound, the C–H in-plane bending vibrations were observed at 1224, 1180 and 1060 cm^{-1} in FT–IR. The theoretically scaled vibrations predicted at the y B3LYP/6-311++G(d,p) level are obtained at 1305, 1274, 1253, 1222, 1209, 1158, 1142 1110 and 1066 cm^{-1}. The C–H out-of-plane bending vibrations are appearing within the region 900–675 cm^{-1} [15]. The vibrations identified at 770, 586, 4985 and 447 cm^{-1} in FT–IR are assigned to C–H out-of-plane bending for MEPCL2.

3.2.2. C–C vibrations

The ring stretching vibrations are useful to identify characteristic of the ring itself. For the title compound, the C=C stretching vibrations are recorded at 1456 and 1388 cm^{-1} in FT–IR with medium intensities. All bands are appearing in the expected range, except first band. Most of the bands are observed with medium and strong intensities. The computed values are at 1459, 1456, 1453, 1441, 1430 and 1427 cm^{-1} at the B3LYP/6-311++G(d,p) level of theory. The other C-C vibrations are computed at 1447, 1444, 1436, 1375 and 1366 cm^{-1}. These vibrations are downshifted when they are compared with those exhibited by aromatic compounds and other C-C vibrations are more shifted with ring C-C vibrations. Only two bands at 992 and 974 cm^{-1} are assigned to C–C-C in-plane bending vibrations of MEPCL2. The two bands are in infrared region with very strong intensities. The computed vibrations are tabulated to C-C-C in-plane and out-of-plane bending vibrations at 1001, 951, 921 and 270, 222 and 266 cm^{-1}.

3.2.3. Methyl group vibrations

For the assignment of CH_3 group frequencies, nine fundamental vibrations can be associated with each CH_3 group. Three stretching, three bending, two rocking modes and single torsional mode describe the motion of the methyl group. In the experimental FT–IR band is observed at 2928 cm^{-1} for MEPCL2 have been assigned to CH_3 symmetric stretching vibration. The CH_3 stretching

vibrations are calculated as 2893, 2916, 2913, 2912, 2908, 2906, 2899, 2894 and 2877 cm^{-1} at the B3LYP/6-311G++(d,p) level of theory. The FT–IR band observed at 1388 cm^{-1} have been assigned to CH_3 in-plane bending vibration for MEPCL2.

3.2.4. P-Cl and P-O vibrations

The experimental P-Cl stretching vibrations are observed in the interval 587–435 cm^{-1}. Also, a band at 447 cm^{-1} is assigned as P-Cl vibration. The calculated P-Cl in-plane and out-of-plane bending vibrations are observed at 387, 233 and 34 cm^{-1}. The P-O phenyl linkage gives rise to two bands. A strong band at 1260-1160 cm^{-1} is mainly due to the stretching of the C-O bond of the phenyl group. Also, the band at 992 cm^{-1} is related to a C-O stretching vibration.

The simulated infrared spectra of MEPCL2 obtained at the HF/6-311G++(d,p) and B3LYP/6-311G++(d,p) levels of theory are shown in Fig. 3.

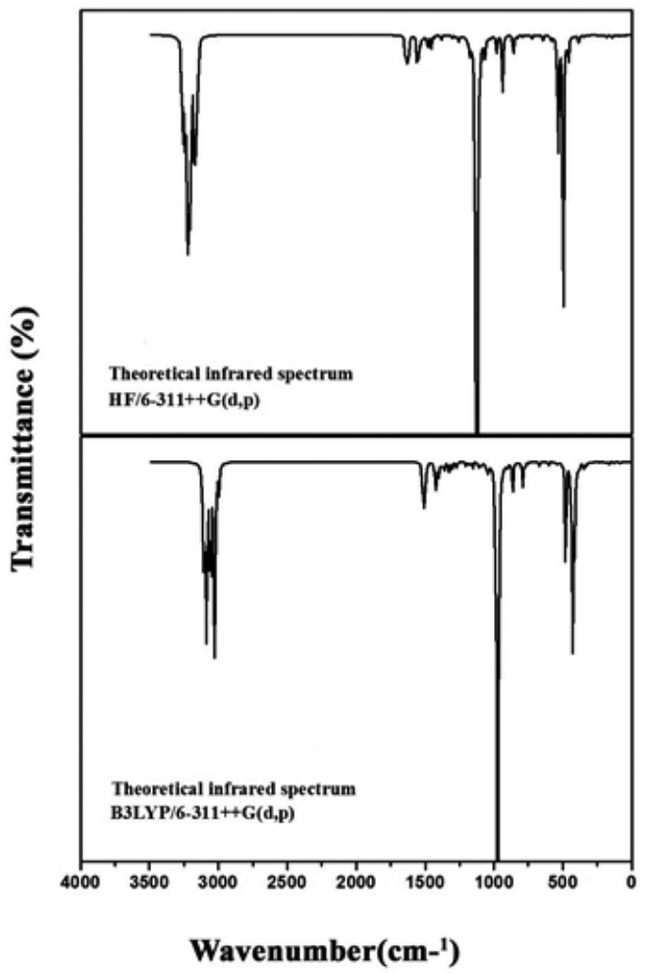

Fig. 3. Computed FT–IR spectra for MEPCL2

3.3. Frontier molecular orbitals (FMOs)

The highest occupied molecular orbital (HOMO) and the lowest-lying unoccupied molecular orbital (LUMO) may describe the electronic transition, non-linear optic properties, and UV–Vis spectra of a molecular system[16]. Also, the energy gap between HOMO and LUMO determines the kinetic stability, chemical reactivity and, optical polarizability and chemical hardness–softness of a molecule[17,18]. The hard molecules are less polarizable than the soft ones because they need big energy to excitation. The electronic calculated through the TD-DFT method. In order to evaluate the energetic behavior of MEPCL2 in the solvent, we carried out calculations considering acetonitrile, water, chloroform and gas phases. The energies of the four molecular orbitals of MEPCL2: the second highest and highest occupied MO's (HOMO and HOMO−1), the lowest and the second lowest unoccupied MO's (LUMO and LUMO+1) were calculated at the TD-DFT/B3LYP/6-311++G(d,p) level of theory and they are reported in Table 3. Also, the 3D plots of the HOMO-1, HOMO, LUMO and LUMO+1 orbitals computed at TD-DFT/B3LYP/6-311++G(d,p) level of theory for MEPCL2 molecule are depicted in Fig. 4. It is clear from this figure that, while the HOMO is localized on almost the whole molecule, LUMO is especially localized on the ring. Also, note that both, the HOMOs and the LUMOs are mostly anti-bonding type orbitals.

The calculated energy values of the HOMO and LUMO energy gaps are 6.3017, 6.3008, 6.3085 and 6.3183 eV in acetonitrile, water, chloroform and gas phases, respectively. Thus, it is clear that the highest energy gap is obtained when chloroform solvent is employed which suggest that MEPCL2 is more chemically stable in such solvent. In view of calculated absorption spectra, the maximum absorption wavelength corresponds to the electronic transition from the HOMO to LUMO with 92% and from the HOMO to LUMO+1 with 9% contribution, see Table 4. The other wavelength, excitation energies, oscillator strength and calculated counterparts with major contributions are listed in Table 4.

Table 3. Computed energy values of MEPCL2 in acetonitrile, water, chloroform and gas.

TD-DFT/B3LYP/ 6-311++G(d,p)	Acetonitrile	Water	Chloroform	Gas
E_{total} (Hartree)	-1729.77	-1729.77	-1729.76	-1729.76
E_{HOMO} (eV)	-7.90	-7.91	-7.89	-7.85
E_{LUMO} (eV)	-1.60	-1.61	-1.58	-1.54
$\Delta E_{HOMO\text{-}LUMO\ gap}$ (eV)	6.30	6.30	6.31	6.32
$E_{HOMO\text{-}1}$ (eV)	-8.05	-8.05	-8.08	-8.19
E_{LUMO+1} (eV)	-1.18	-1.18	-1.58	-1.14
$\Delta E_{HOMO\text{-}1\text{-}LUMO+1\ gap}$ (eV)	6.87	6.86	6.50	7.05
$E_{HOMO\text{-}2}$ (eV)	-8.18	-8.18	-8.21	-8.34
E_{LUMO+2} (eV)	-0.24	-0.24	-0.28	-0.43
$\Delta E_{HOMO\text{-}2\text{-}LUMO+2\ gap}$ (eV)	7.94	7.94	7.93	7.92

Note that the calculations of the molecular orbital show that the visible absorption maxima of MEPCL2 corresponds to the electron transition between frontier orbitals such as translation from HOMO to LUMO, see Table 4. The calculated absorption spectra showed five bands at 227.8, 220.9, 211.5, 208.9 and 201.6 nm for acetonitrile and at 227.2 nm in the experimental UV spectrum with maximum absorbance in the same solvent. In chloroform, water and gas phases, the theoretical maximum absorption bands are predicted at 228.2, 227.8 and 226.2 nm, respectively. All the maximum absorption bands are coming from HOMO to LUMO transition with energy contribution about 96 to 97 %. The next maximum peaks are predicated on HOMO-1 to LUMO+1 in all UV spectra with 80 to 90% around 200 nm. In Fig. 5 are shown the theoretical UV spectra obtained at the TD-DFT/6-311++G(d,p) level of theory, in all cases, it is possible to observe that the maximum absorbance is in the range 226-228 nm.

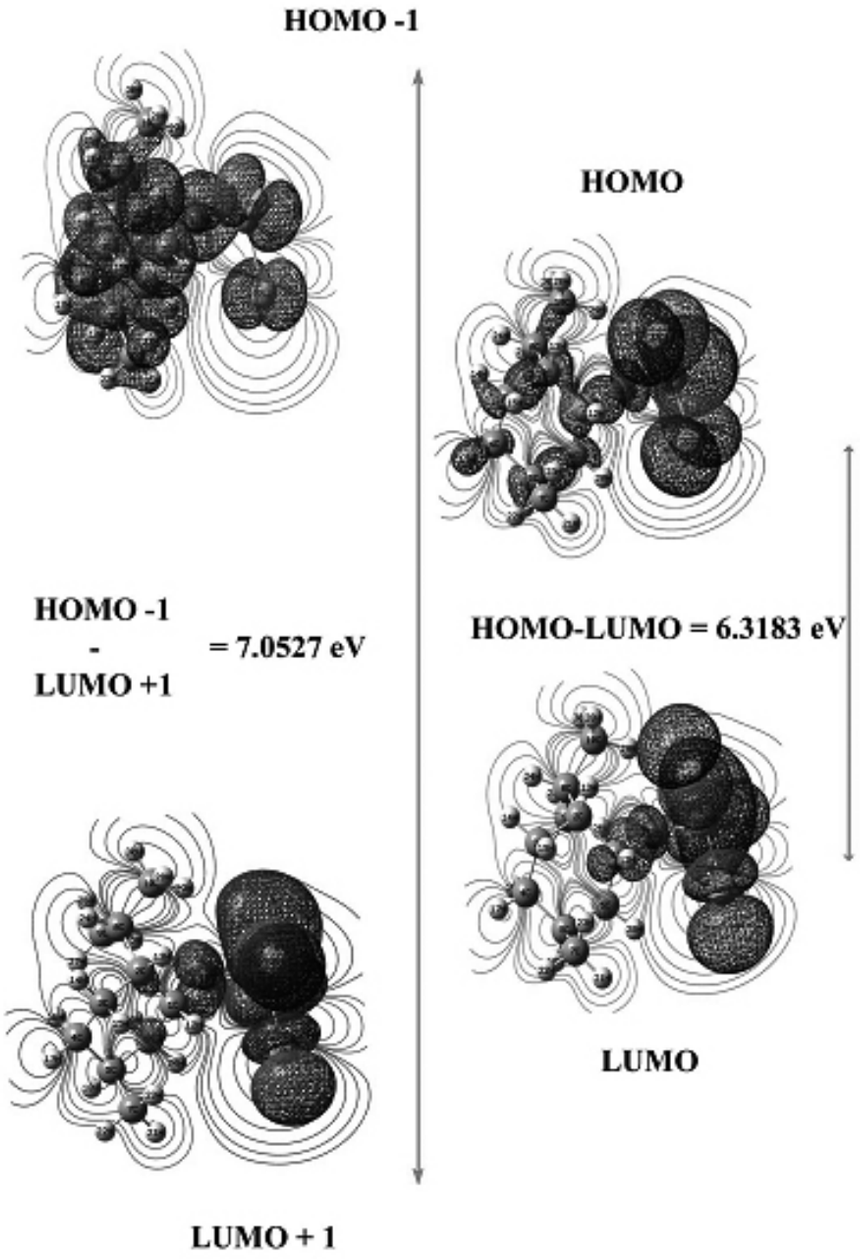

Fig. 4. 3D view of HOMO and LUMO diagram with energy gaps.

3.4. ^{1}H and ^{13}C NMR spectra from quantum calculations

The theoretical values for ^{1}H and ^{13}C NMR of MEPCL2 are given in Table 5. The theoretical ^{1}H and ^{13}C NMR chemical shifts of MEPCL2 have been compared with the experimental data measured in water and $CDCl_3$ solvents.

A comparison, between the experimental and computed ^{13}C NMR spectra of MEPCL2, indicates an increase in the value of the chemical shifts of the carbon atoms C1 and C2 of cyclohexane, due to heavy substitutions, which is caused by the electronic charge distribution around of these carbon atoms.

The hydrogen peaks in the cyclohexane are observed experimentally from 2.228 to 1.331 ppm, while that the evaluated at the B3LYP/6-311+G (d,p) level of theory are in the range 2.238 - 1.174 ppm.

The methyl hydrogen atom H22 peak identified at 0.809 ppm is the lowest chemical shift among the entire hydrogen atoms. Probably, it is because of its electronic interaction with other atoms is lesser. The correlation graphs of the experimental and theoretical ^{1}H, and ^{13}C NMR chemical shift are presented as supplementary material in Fig 6. A good correlation between predicted and observed ^{13}C and ^{1}H NMR chemical shifts is found. Moreover, the slope and intercept of the least-square, correlation lines were used to scale the GIAO isotropic absolute shielding constants. From Fig. 6 it is clear that the solvent water shows more deviation that the observed in the $CDCl_3$ solvent. The relation is usually linear and described by the following equations (1-4):

Table 4. Theoretical electronic absorption spectra of MEPCL2 excitation energies E (eV), (absorption wavelength λ (nm), and oscillator strengths (*f*) using TD-DFT/B3LYP/6-311++G(d,p) method.

Solvent	Energy (eV)	Wavelength	Oscillator strength	Major contribution
Acetonitrile	5.4418	227.8	0.0794	HOMO->LUMO (96%)
	5.6102	220.9	0.0005	H-2->LUMO (10%), H-1->LUMO (80%)
	5.8609	211.5	0.0014	H-2->LUMO (84%), H-1->LUMO (11%)
	5.9338	208.9	0.0332	H-5->LUMO (10%), H-4->LUMO (15%), HOMO->L+1 (69%)
	6.1502	201.6	0.0558	H-1->L+1 (87%)
Water	5.4427	227.8	0.0789	HOMO->LUMO (96%)
	5.6072	221.1	0.0005	H-2->LUMO (10%), H-1->LUMO (80%)
	5.8559	211.7	0.0014	H-2->LUMO (84%), H-1->LUMO (11%)
	5.9353	208.9	0.0330	H-5->LUMO (13%), H-4->LUMO (11%), HOMO->L+1 (70%)
	6.1475	201.7	0.0554	H-1->L+1 (87%)
Chloroform	5.4331	228.2	0.0839	HOMO->LUMO (97%)
	5.6409	219.8	0.0005	H-1->LUMO (81%)
	5.9147	209.6	0.0095	H-2->LUMO (67%), HOMO->L+1 (18%)
	5.9202	209.4	0.0260	H-4->LUMO (19%), H-2->LUMO (18%), HOMO->L+1 (50%)
	6.1769	200.7	0.0579	H-1->L+1 (84%)
Gas	5.4788	226.2	0.0579	HOMO->LUMO (96%)
	5.7101	217.1	0.0612	H-1->LUMO (81%)
	5.9263	209.2	0.0002	H-3->LUMO (24%), HOMO->L+1 (55%)
	6.0786	203.9	0.0146	H-2->LUMO (89%)
	6.2299	199.0	0.0003	H-1->L+1 (80%)

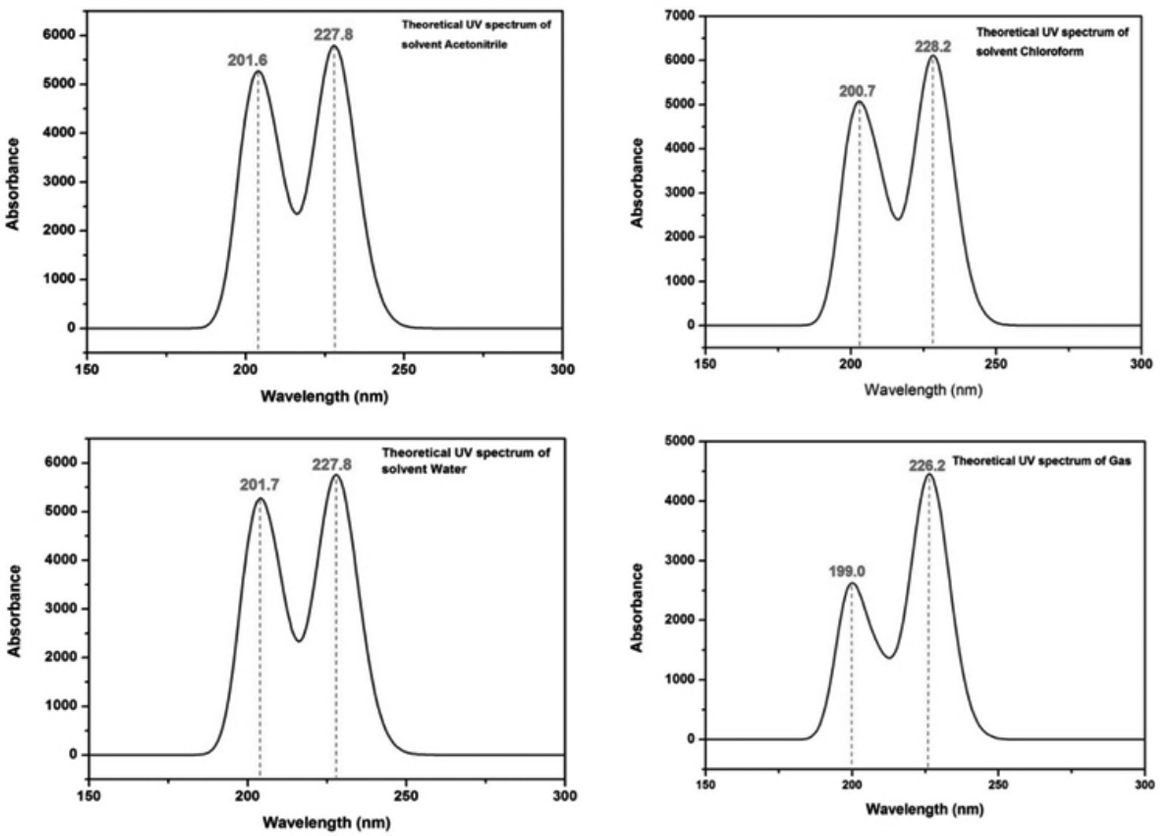

Fig. 5. Computed UV–Vis graphs in different solvent for MEPCL2.

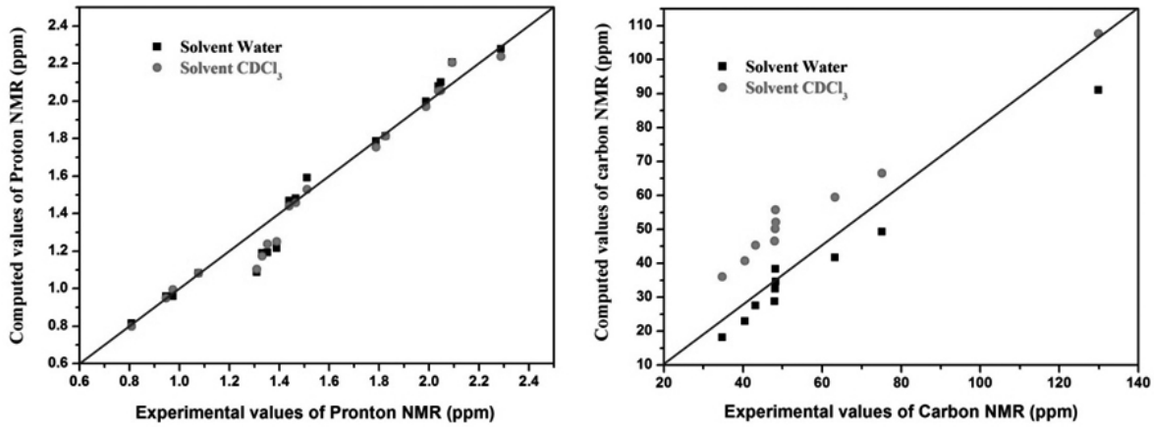

Fig. 6. Correlation Proton and Carbon NMR between experimental and computed data.

Proton NMR

$\nu_{cal.} = -0.1286 + 1.06991\ \nu_{exp.}$ ($R^2 = 0.96503$) in solvent water (1)

$\nu_{cal.} = -0.0923 + 1.03958\ \nu_{exp.}$ ($R^2 = 0.97219$) in solvent $CDCl_3$ (2)

Carbon NMR:

$\nu_{cal.} = -3.86793 + 0.73135\ \nu_{exp.}$ ($R^2 = 0.97407$) in solvent water (3)

$\nu_{cal.} = 14.31258 + 0.0.72025\ \nu_{exp.}$ ($R^2 = 0.97442$) in solvent $CDCl_3$ (4)

These results indicate that the calculations performed at the B3LYP/6-311++G(d,p) predicted adequately the experimental behavior of the ^1H and ^{13}C NMR spectra of MEPCL2.

3.5. Global Chemical Reactivity of MEPCL2

The reactivity of a molecular system can be analyzed employing the global reactivity descriptors derived from the DFT theory, which are evaluated through the total energies of the neutral, anionic and cationic systems. Thus, the ionization potential is determined from the energy difference between the energy of the compound derived from electron-transfer (radical cation) and the respective neutral compound; $IP = E_{cation} - E_n$; while the electron affinity is evaluated as the energy difference between the neutral molecule and the anion molecule: $EA = E_n - E_{anion}$. According to the Koopmans' theorem, in HF calculations, ionization potentials (IP) and electron affinities (EA) may be approximated to the HOMO and LUMO's energies respectively. On the other hand, the validity of the Koopmans' theorem within the DFT approximation is controversial, nonetheless, it has been shown that the Khon-Sham orbitals produce DFT reactivity descriptors that correlate quite well with the reactivity descriptors obtained from Hartree-Fock calculations[19]. Thus, in the present work, we decided to employ the second approximation. Additionally, from IP and EA values it is possible to evaluate the electronegativity (χ), hardness (η), softness (ζ), and electrophilicity index (ψ) of the molecular system, through the equations (5-8)[20]:

$$\text{Electronegativity } (\chi): \mu \approx -\chi = -\frac{IP+EA}{2} \quad (5)$$

$$\text{Chemical hardness } (\eta) \approx \frac{IP-EA}{2} \quad (6)$$

$$\text{Softness } (\zeta) = \frac{1}{2\eta} \quad (7)$$

$$\text{Electrophilicity index } (\psi) = \frac{\mu^2}{2\eta} \quad (8)$$

The values of electronegativity, chemical hardness, softness, electrophilicity index and dipolar moment are reported in Table 6, in the solvents acetonitrile, water, chloroform and gas phases.

Table 5. Experimental and theoretical probable ^1H and ^{13}C NMR isotropic chemical shifts (with respect to TMS and in Water and $CDCl_3$ solution) of MEPCL2 compound.

Atom	Experimental (ppm)[7]	Theoretical (B3LYP) (ppm)	
		Water	$CDCl_3$
H12		5.123	5.085
H19	2.288	2.277	2.238
H13	2.092	2.207	2.206
H15	2.047	2.100	2.056
H18	2.038	2.080	2.053
H16	1.988	1.998	1.970
H20	1.826	1.814	1.813
H24	1.788	1.786	1.754
H27	1.511	1.591	1.529
H23	1.466	1.480	1.459
H14	1.439	1.468	1.441
H26	1.390	1.214	1.250
H29	1.353	1.192	1.237
H17	1.331	1.189	1.174
H28	1.310	1.087	1.103
H25	1.077	1.082	1.082
H21	0.975	0.958	0.995
H30	0.947	0.958	0.950
H22	0.809	0.814	0.799
C1	129.88	91.018	107.714
C2	75.14	49.268	66.567
C8	63.21	41.677	59.452
C6	48.24	38.348	55.768
C5	48.26	34.568	52.099
C3	48.15	32.526	50.223
C4	48.01	28.808	46.545
C10	43.19	27.558	45.318
C9	40.47	22.992	40.696
C7	34.74	18.220	35.978

Table 6. Computed electronegativity, chemical hardness-softness, and dipolar moment of MEPCL2 in acetonitrile, water, chloroform and gas phases.

B3LYP/ 6-311++G(d,p)	Acetonitrile	Water	Chloroform	Gas
Electronegativity χ (eV)	4.75	4.76	4.74	4.70
Chemical hardness η (eV)	3.15	3.15	3.15	3.16
Softness ζ (eV)$^{-1}$	0.16	0.16	0.16	0.16
Electrophilicity index ψ (eV)	3.59	3.59	3.55	3.49
Dipolar moment (Debye)	3.87	3.89	3.67	3.15

From these values, observe that the values of χ, η, ζ, and ψ are similar, this means that MEPCL2 is showing the same global chemical behavior in the different solvents, but it is clear that the dipolar moment has different values which depend on the solvent in where the molecule is immersed. The above mentioned is indicative of the presence of different intramolecular interactions between the solvent and MEPCL2.

3.6. Local reactivity of MEPCL2 from Molecular Electrostatic Potential

In the present study, the molecular electrostatic potential (MESP) of MEPCL2 is plotted in order to analyze its local reactivity, see Fig. 7. The MESP is a plot of the electrostatic potential mapped onto an electron density isosurface and is useful to identify electrophilic and nucleophilic regions around the molecule. In the majority of the MESP, while the maximum negative region, which preferred site for electrophilic attack indications as red color, the maximum positive region which preferred site for nucleophilic attack symptoms as blue color. The electrophilic attack is more around phosphorous and carbon atoms. It is extended around chlorine atoms. Similarly, nucleophilic attacks are shown in hydrogen atoms and more in methyl group substitutions. The different values of the electrostatic potential at the MESP surface are represented by different colors; red, blue and green represent the regions of most negative, most positive and zero electrostatic potential, respectively. The color code of these maps is in the range between -0.02335 e. (deepest red) to 0.02335 e (deepest blue) in the compound, where blue indicates the strongest attraction and red indicates the strongest repulsion[21-26].

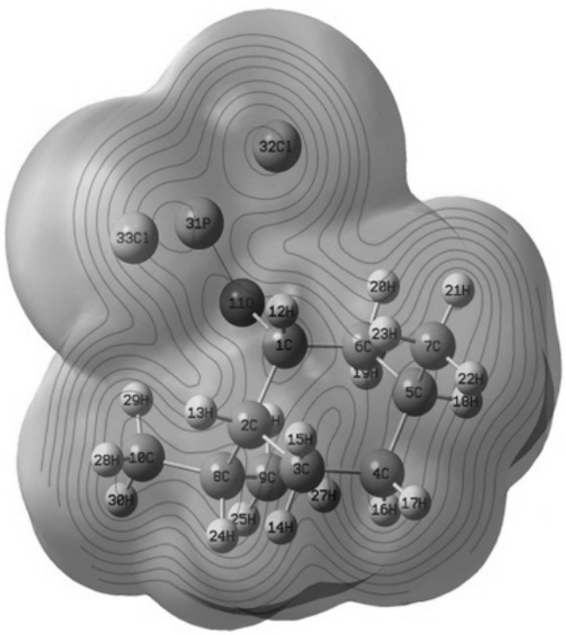

Fig. 7. Molecular electrostatic potential (MESP) of MEPCL2

CONCLUSIONS

In this work, the geometric parameters and vibrational frequencies of the mentoxy dichloro phosphorous ($C_{10}H_{19}OPCl_2$) were evaluated at the HF/6-311++G(d,p) and B3LYP/6-311++G(d,p) levels of theory. In comparison to the experimental results, the computed vibrational frequencies obtained by the B3LYP method are better than those obtained by the Hartree–Fock method. Fundamental vibrations with their mode were fully discussed in order to give a better understanding of the electronic structure of MEPCL2. The HOMO–LUMO gaps and implications of the electronic transitions were examined. The kinetic stability, chemical reactivity, optical polarizability, and chemical hardness–softness were discussed by frontier molecular orbital gaps. With orbital analysis, it has been suggested that MEPCL2 is more stable in chloroform than in other solvents. The ^{1}H, and ^{13}C NMR recorded and isotropic chemical shifts were calculated and they compare favorably well with the experimental results. The evaluation of the global reactivity descriptors suggests a similar chemical behavior of MEPCL2 in the different solvents analyzed. The molecular electrostatic potential isosurface provides a visual performance of the chemically active sites and comparative reactivity of atoms. Thus the present investigation provides complete vibrational assignments, structural information, chemical shifts and electronic properties of the MEPCL2.

ACKNOWLEDGEMENTS

The authors gratefully acknowledge the financial support from the Research Council of Imam Khomeini International University. Also, the authors greatly appreciate Prof. M. Govindarajan for valuable comments and discussions. LHMH expresses his gratitude to the Mexican National Council for Science and Technology (CONACYT) for financing this work through the Research Project Grant 257823 and to the Universidad Autónoma del Estado de Hidalgo. The authors gratefully acknowledge too the financial support of research Direction UCSC.

REFERENCES

1. Sengupta, S. K., Pandey, O. P., Rao, G. P., Vishen, P.: Metal Based Drugs. 8, 293 (2002)
2. Suarez, P., Dullius, J.E. L., Einloft, S., De Souza, R., Dupont, R.: J. Inorg. Chim. Acta. 255, 207–209 (1997)
3. Boon, A., Levisky, J. L., Pflug, L., Wilkes, J. S.: J. Inorg. Chem. 51, 480–483 (1986)
4. Yanes, E. G., Gratz, S. R., Baldwin, M. J., Robinson, S.E., Stalcup, A. M.: Anal. Chem. 73, 3838 (2001)
5. Racke, K.D.: Degradation of organophosphorus insecticides in environmental matrices. in: Chambers, J.E., Levi, P.E. (eds.), Organophosphates: Chemistry, Fate, and Effects. Academic Press, San Diego. 47–73 (1992).
6. Quin, L. D.: A Guide to Organophosphorus Chemistry; John Wiley & Sons, (2000).
7. Mendoza-Huizar, L.H., J. Mex. Chem. Soc, 5(4) 416 (2014)
8. Gaussian 03, Revision C.02, Frisch, M. J.; Trucks, G. W.; Schlegel, H. B.; Scuseria, G. E.; Robb, M. A.; Cheeseman, J. R.; Montgomery, Jr., J. A.; Vreven, T.; Kudin, K. N.; Burant, J. C.; Millam, J. M.; Iyengar, S. S.; Tomasi, J.; Barone, V.; Mennucci, B.; Cossi, M.; Scalmani, G.; Rega, N.; Petersson, G. A.; Nakatsuji, H.; Hada, M.; Ehara, M.; Toyota, K.; Fukuda, R.; Hasegawa, J.; Ishida, M.; Nakajima, T.; Honda, Y.; Kitao, O.; Nakai, H.; Klene, M.; Li, X.; Knox, J. E.; Hratchian, H. P.; Cross, J. B.; Bakken, V.; Adamo, C.; Jaramillo, J.; Gomperts, R.; Stratmann, R. E.; Yazyev, O.; Austin, A. J.; Cammi, R.; Pomelli, C.; Ochterski, J. W.; Ayala, P. Y.; Morokuma, K.; Voth, G. A.; Salvador, P.; Dannenberg, J. J.; Zakrzewski, V. G.; Dapprich, S.; Daniels, A. D.; Strain, M. C.; Farkas, O.; Malick, D. K.; Rabuck, A. D.; Raghavachari, K.; Foresman, J. B.; Ortiz, J. V.; Cui, Q.; Baboul, A. G.; Clifford, S.; Cioslowski, J.; Stefanov, B. B.; Liu, G.; Liashenko, A.; Piskorz, P.; Komaromi, I.; Martin, R. L.; Fox, D. J.; Keith, T.; Al-Laham, M. A.; Peng, C. Y.; Nanayakkara, A.; Challacombe, M.; Gill, P. M. W.; Johnson, B.; Chen, W.; Wong, M. W.; Gonzalez, C.; and Pople, J. A.; Gaussian, Inc., Wallingford CT, 2004.
9. Karabacak, M., Kurt, M.: Spectrochim. Acta A. 71, 876–883 (2008).
10. Jamróz, M.H.: Vibrational Energy Distribution Analysis, VEDA 4, Warsaw, (2004).
11. Kemp, W.: Organic Spectroscopy, Mac Millan Press Ltd., London, (1991).
12. Shishkov, I.F., Sadova, N.I., Novikov, V.P., Vilkov, L.V., Strukt. Khim, Zh.: 25 (1984) 98–102.

13. Sinha, L., Karabacak, M., Narayan, V., Cinar, M., Prasad, O.: Spectrochim. Acta
14. 109A, 298–307 (2013).
15. Socrates, G.: Infrared and Raman Characteristic Group Frequencies – Tables and Charts. third ed., Wiley, New York, (2001).
16. Karabacak, M., Karagoz, D., Kurt, M.: J. Mol. Struct., 892, 25–31 (2008).
17. Rani, A.U., Sundaraganesan, N., Kurt, M., Cinar, M., Karabacak, M.: Spectrochim. Acta A 75, 1523–1529 (2010).
18. Balachandran, V., Lakshmi, A., Janaki, A.: Spectrochimica Acta A 81, 1–7 (2011)
19. Bevan Ott, J., Boerio-Goates, J.: Calculations from Statistical Thermodaynamics, Academic Press, (2000).
20. Martínez-Araya, J.I., Salgado-Morán, G., Glossman-Mitnik, D. J. Chem., 2013, 1 (2013)
21. Krishnakumar, V., John Xavier, R.: Indian J. Pure Appl. Phys., 41, 597 (2003).
22. Lashgari, A., Ghamami, S., Salgado-Morán, G., Ranirez-Tagle, R., Lorena Gerli – Candia, Journal of the Chilean Chemical Society, 61(1), 2821-2827 (2016).
23. Lashgari, A., Ghammamy, S., Ramirez-Tagle, R., Salgado-Moran, G., Journal of Structural Chemistry, 56(8), 1505-1513, (2015).
24. Ghamami, S., Shahbazkhany, S., Lashgari, A., International Journal of Pure and Applied Chemistry, 9(1-2), 57-62 (2014).
25. Ghamami, S., Lashgari, A., Open Access Library Journal, 1: e422 (2014).
26. Lashgari, A., Ghammamy, S., Shahsavari, M., Asian Journal of Research in Chemistry, 7(7), 677-680 (2014).